The Slab Geometry Laser—Part I: Theory

J. M. EGGLESTON, T. J. KANE, K. KUHN, J. UNTERNAHRER,
AND R. L. BYER, MEMBER, IEEE

Abstract—Slab geometry solid-state lasers offer significant performance improvements over conventional rod geometry lasers. We present a detailed theoretical description of the thermal, stress, and beam propagation characteristics of a slab laser. Our analysis includes consideration of the effects of the zig-zag optical path which eliminates thermal and stress focusing and reduces residual birefringence.

I. Introduction

SOLID-STATE lasers traditionally are fabricated in the shape of a long thin rod. Under operating conditions the thermally loaded laser host medium exhibits optical distortions which include thermal focusing, stress induced biaxial focusing, and stress induced birefringence [1]-[4]. These thermally induced effects severely degrade the optical quality of the laser beam and eventually limit the laser output power.

The limitations imposed by the rod geometry have long been recognized. As early as 1969 Martin and Chernoch [5] proposed using a rectilinear slab geometry to eliminate stress induced biaxial focusing and birefringence. They also realized that a zig-zag optical path, confined to the slab by total internal reflection, could be used to eliminate thermal and stress induced cylindrical focusing. The advantages of the slab configuration are the combination of two ideas: the elimination of stress induced birefringence by geometry and the elimination of thermal and stress induced focusing by optical propagation along a zig-zag path.

The proposed face pumped, zig-zag optical path, slab laser was investigated in 1972 using Nd:Glass [6], [7] and Nd:SOAP [8] as host materials. The studies were extended in 1975 to include Nd:YAG [9]. These investigations demonstrated the potential for improvements in laser performance provided by the slab geometry. Although these early results were published [10], engineering difficulties and fabrication expense held back wider use of the slab concept. Work is continuing on both Nd:Glass and Nd:YAG [11], [12] slab laser systems.

There is an increasing interest in solid-state laser sources and in the improved performance offered by the slab geometry. We have carried out extensive theoretical and experimental studies of the slab approach using a Stanford test-bed Nd:Glass laser system. Preliminary results have been published [13], [14] and the work has been extended to crystalline laser media including Nd:YAG and Nd:GGG [15].

Improvements in solid-state laser engineering [16], [17] and increased optical fabrication capability, at lower cost, have enabled many of the earlier difficulties associated with the slab geometry to be overcome. However, to date, the theory of the zig-zag path slab geometry laser has not been published, thus preventing optimum laser design.

This paper presents a theoretical study (Part I) of the slab geometry solid-state laser concept. The theory of thermal stress analysis in an isotropic solid is introduced and the thermal and stress induced focusing and birefringence are discussed for both the rod and slab geometry. Optical propagation through a rod and slab is analyzed and compared. Experimental results verify that, as expected, the zig-zag optical path eliminates first-order thermal and stress induced focusing. The zig-zag optical path also reduces stress induced birefringence and leads to high average power laser operation limited only by stress induced fracture of the laser medium. Scaling laws for slab geometry lasers are derived and discussed.

II. Thermal Stress Analysis

A. Introduction

The theoretical background necessary to analyze thermal stress induced optical effects in a laser rod and slab are developed in this section. The results are applied to rod and slab configuration media. The analysis is limited to bulk effects in a semi-infinite slab. It does not include end effects which are difficult to determine analytically. A list of variables is included in Table I.

B. Heat Flow

The problem of heat flow in a laser medium is well understood and solutions for the rod and slab geometry have been given previously [1]-[4]. The equations are presented here for completeness.

Consider the rectangular slab of isotropic material shown in Fig. 1(a), with a thermal power loading per unit volume $Q(x, y, t)$. Here, $Q(x, y, t)$, (W/cm^3) is assumed to be independent of z. If the faces normal to the z direction (z faces) are not cooled and the thermal boundary conditions on the x and y faces are independent of z, the temperature distribution in the medium reduces to a two-dimensional problem governed by the time dependent equation

$$\frac{C\rho}{k}\dot{T} = \nabla^2 T + \frac{Q}{k} \tag{1}$$

where k is the thermal conductivity $(W \cdot cm^{-1} \cdot K^{-1})$, C is the specific heat $(J \cdot g^{-1} \cdot K^{-1})$, ρ is the mass density $(g \cdot cm^{-3})$, and T is the temperature (K). For CW pumping or for pulsed

Manuscript received April 12, 1983; revised November 10, 1983. This work was supported in part by the Swiss Institute of Nuclear Research, by the U.S. Army under Contract DAAG20-81-C-0038, by the Department of Energy under Contract DOE3818 301, and by the National Aeronautics and Space Administration under Contract NAG/NASA 5-220.

J. M. Eggleston is with Mathematical Sciences N.W. Inc., Bellevue, WA 98004.

T. J. Kane, K. Kuhn, and R. L. Byer are with the Edward L. Ginzton Laboratory of Physics, Stanford University, Stanford, CA 94305.

J. Unternahrer is with the Swiss Nuclear Institute, Villigen, Switzerland.

0018-9197/84/0300-0289$01.00

TABLE I
LIST OF VARIABLES

$\bar{\bar{B}}, B_{ijkl}, B_{\perp}, B_{\parallel}$	stress optic tensor, tensor components, and perpendicular and parallel components	$\bar{r}$	position vector
C	specific heat	t	slab thickness
d	rod diameter	T	temperature
dn/dT	change in index of refraction with temperature	T'	deviation from average slab temperature
E	Young's modulus	$\dot{T}$	time derivative of temperature
E_x, E_y, E_+, E_-	electric field components	T_a	average value of temperature
E_{st}, E_{sat}	stored energy density, saturation energy fluence	$\bar{U}$	vector displacement function
$f_\xi, \xi = (r, \theta, x, y)$	focal length	U_i	the ith component of $\bar{U}$
G_0	unsaturated gain	$\hat{u}$	normal unit vector
g_0	unsaturated gain coefficient	v	volume
J	total stored upper level energy	w	slab width
k	thermal conductivity	X_i	the ith Cartesian coordinates
k_v	vacuum wavenumber	x, y, z	Cartesian coordinator
l	slab length	α	thermal expansion coefficient
l_p	gain length in the slab	$\alpha_\xi\ \xi = (r, \theta, x, y)$	index of refraction gradient parameter
M_s	material constant defined by $(1 - \nu)k/\alpha E$	ϵ, ϵ_{ij}	strain and components of strain
$\bar{\bar{n}}, n_{ij}, n_{\xi\xi}, \xi = (r, \theta, x, y)$	index of refraction tensor, tensor component	Δn_s	change in index of refraction
n^0	initial index of refraction value	θ(rod)	cylindrical coordinate
n_a	average index of refraction	θ(slab)	angle with respect to the z axis
N	number of zig-zag bounces	η_{ex}	extraction efficiency
P_a	average thermal power loading	ν	Poisson's ratio
$P_{\text{out}}^{\text{ave}}$	average laser output power	ϕ	Airy stress potential
Q	thermal loading power per unit volume (W/cm^3)	σ, σ_{ij}	stress tensor and components
$R, R_i\ i = (\theta, r, x, y)$	optical rays	$\sigma_{\xi\xi}\ \xi = (r, \theta, x, y, z)$	stress components
R	repetition rate	$\sigma_{\max}$	stress fracture limit
R_s	thermal stress resistance parameter	σ_s	surface stress
r	radial coordinate	ρ	mass density
		τ	thermal relaxation time
		λ	surface heat transfer coefficient
		χ	heat dissipated per stored upper level energy

pumping with an inverse repetition rate that is much less than the thermal relaxation time constant,

$$\tau = \frac{C\rho}{k}\left(\frac{t}{\pi}\right)^2 \tag{2}$$

where t is the thickness in the y direction. Equation (1) reduces to the time independent equation

$$\nabla^2 T(x, y) = \frac{-Q(x, y)}{k}. \tag{3}$$

The thermal boundary conditions at the surface, denoted by S, are given by

$$k\left.\frac{dT}{d\bar{u}}\right|_S = k_c \frac{dT}{d\bar{u}} \qquad T|_S = T_c|_S \tag{4a}$$

where T_c is the coolant temperature and k_c is the thermal conductivity of the coolant. In the case of a flowing coolant with a boundary layer, the thermal boundary condition is given by Newton's law of heat transfer

$$k\left.\frac{dT}{d\bar{u}}\right|_S = \lambda(T_c - T|_S) \tag{4b}$$

where λ is the surface heat transfer coefficient [16] ($W \cdot cm^{-2} \cdot K^{-1}$) and $\bar{u}$ is the outward normal to the surface S. Given the value of $Q(x, y)$ there are well known methods of solving (3) and (4) for the temperature distribution $T(x, y)$ [18].

C. Stress and Strain

In the absence of thermal loading, the slab is assumed to be stress-free and not constrained by external forces. When the temperature changes from its original value the mass elements are displaced. Let the vector function $\bar{U}(\bar{r})$ represent this displacement such that the mass element at position $\bar{r}$ is displaced to $\bar{r} + \bar{U}(\bar{r})$. The strain tensor is defined as

$$\epsilon_{ij} = \frac{1}{2}\left(\frac{\partial U_i}{\partial X_j} + \frac{\partial U_j}{\partial X_i}\right). \tag{5}$$

Hooke's law requires that the strain tensor components be linearly related to the stress tensor components by [18]

$$\epsilon_{ij} = \frac{1}{E}\left\{(1 + \nu)\,\sigma_{ij} - \nu(\sigma_{xx} + \sigma_{yy} + \sigma_{zz})\,\delta_{ij}\right\} + \alpha T \delta_{ij} \tag{6}$$

where E is Young's modulus (Pa), ν is Poisson's ratio, α is the thermal expansion coefficient, T is the temperature, and δ_{ij} is the Kronecker delta. The on-diagonal stress tensor elements (σ_{ii}) are compressive or expansive forces, and the off-diagonal elements ($\sigma_{ij}\ i \neq j$) are the shear forces in the i–j plane. Assuming that there are no internal forces, the balancing of forces

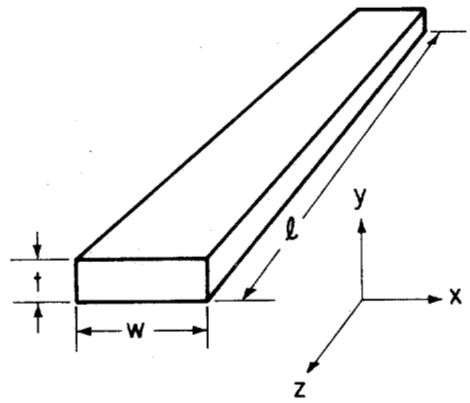

(a)

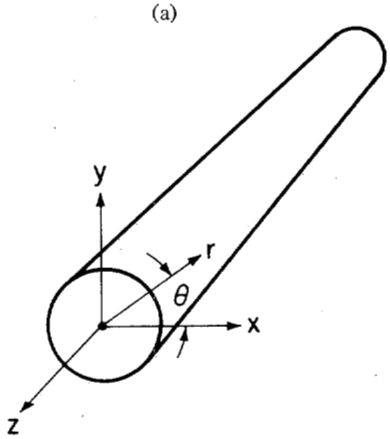

(b)

Fig. 1. (a) The slab geometry system with a rectangular slab of isotropic material of thickness t, width w, and length l. The slab is assumed to be pumped and cooled through the faces normal to the y direction (the y faces). Optical propagation is a zig-zag path in the z direction. (b) The rod geometry system with radial distance r and angle between the radial direction and the x axis θ.

requires

$$\sum_j \frac{\partial \sigma_{ij}}{\partial X_j} = 0. \tag{7a}$$

The free surface boundary conditions are

$$\sum_j \sigma_{ij} u_j = 0 \tag{7b}$$

where u_j is the jth component of the outward normal surface vector. Equations (7a) and (7b) do not specifiy a unique solution for the stress tensor components σ_{ij}. A unique solution is specified if we also require the existence of the function $\bar{U}(\bar{r})$ which is related to the σ_{ij} through (5) and (6). This requirement gives rise to the compatibility equations which are derived below for the two-dimensional case.

An alternate way to find a unique solution for the σ_{ij} is to invert (6) yielding

$$\sigma_{ij} = \frac{E}{1-\nu}\left\{\epsilon_{ij} + \frac{\nu}{1-2\nu}(\epsilon_{xx}+\epsilon_{yy}+\epsilon_{zz})\delta_{ij} - \frac{1+\nu}{1-2\nu}\alpha T\delta_{ij}\right\}. \tag{8}$$

Using (5) to replace ϵ_{ij} with partial derivatives of $\bar{U}(\bar{r})$, these expressions can be used to eliminate the σ_{ij} in (7a). The resulting equation is

$$\nabla^2 \bar{U} + \frac{1}{1-2\nu}\bar{\nabla}(\bar{\nabla}\cdot\bar{U}) = \frac{2(1+\nu)}{1-2\nu}\alpha\bar{\nabla}T \tag{9}$$

with the boundary conditions

$$(\bar{u}\cdot\bar{\nabla})U_i + \frac{2u_i\nu\bar{\nabla}\cdot\bar{U}}{1-2\nu} + \sum_j u_j\frac{\partial U_j}{\partial X_i} = \frac{2(1+\nu)}{1-2\nu}\bar{u}_i\alpha T. \tag{10}$$

The solution of (9), that meets the boundary conditions given by (10), is unique except for a rigid body translation. Equation (9) with the boundary conditions is a very difficult problem to solve even on a large computer. In order to reduce this three-dimensional problem to a two-dimensional one, we introduce the plane strain approximation.

It is a common approximation in stress/strain problems of the type under consideration to use the plane strain approximation. This approximation assumes that the problem is independent of one dimension. Before invoking this approximation a few preliminary steps are necessary.

Consider the solution of (9) and (10) for a change in temperature given by

$$T(x,y) = T_a + T'(x,y) \tag{11a}$$

where

$$\int_A T'(x,y)\,dxdy = 0. \tag{11b}$$

Here, A is the cross-sectional area and T_a is the average temperature of the slab.

Due to the linearity of (9) and (10) the displacement induced by the temperature distribution $T(x,y)$ is the superposition of the displacement induced by the uniform temperature T_a and the temperature distribution $T'(x,y)$. The solution for the displacement induced by T_a is $\bar{U}(\bar{r}) = \alpha T_a\bar{r}$, which may be verified by direct substitution into (9) and (10). This solution yields a uniform strain throughout the slab and zero stress [see (5) and (7)].

The problem is to determine the stress and strain induced by $T'(x,y)$. Since $T'(x,y)$ has a zero mean temperature, the average length in the z direction, as well as the volume of the slab, is independent of $T'(x,y)$. The principle of St. Venant [19] can be invoked to show that the displacements in the z direction disappear except near the z faces. Thus in the region that is one or two slab thicknesses away from the z faces, the z component of strain is essentially zero. The plane strain approximation entails setting ϵ_{zz} to zero everywhere in the slab. The plane strain approximation applies to the present problem since the slab extent in the z direction is assumed to much greater than in the y direction.

A consequence of this approximation is that end effects are not included in this model.

Setting ϵ_{zz} to zero means that the displacement $\bar{U}(\bar{r})$ must be independent of z, that is $\bar{U}(\bar{r}) = \bar{U}(x,y)$. Due to the reflection symmetry through the xy plane, it is evident that ϵ_{yz} and ϵ_{xz} are also zero throughout the slab. Thus the equation governing $\bar{U}(\bar{r})$ is reduced from three to two dimensions.

Under the plane strain approximation, (9) and (10) do not

change form. However, all operators are two-dimensional instead of three-dimensional. The problem of solving for the stress now has been reduced to solving for two coupled functions U_x and U_y on a section of a plane. It should be noted that, in general, the curl of $\bar{U}(x, y)$ is not zero and that potential functions such as those of electrostatics cannot be used to solve $\bar{U}(x, y)$. In order to use a scalar potential function, it is necessary to formulate the problem in terms of the two-dimensional stress distribution.

When ϵ_{zz}, ϵ_{xz}, and ϵ_{yz} are set to zero in the expression for Hooke's law, (6) or (8), the stress/strain relationships may be rewritten as

$$\sigma_{xz} = \sigma_{yz} = 0 \tag{12a}$$

$$\sigma_{zz} = \nu(\sigma_{xx} + \sigma_{yy}) - E\alpha T' \tag{12b}$$

$$\epsilon_{xx} = \frac{1}{E}\left\{(1-\nu^2)\sigma_{xx} - \nu(1+\nu)\sigma_{yy}\right\} + (1+\nu)\alpha T' \tag{12c}$$

$$\epsilon_{yy} = \frac{1}{E}\left\{(1-\nu^2)\sigma_{yy} - \nu(1+\nu)\sigma_{xx}\right\} + (1+\nu)\alpha T' \tag{12d}$$

$$\epsilon_{xy} = \frac{(1+\nu)}{E}\sigma_{xy}. \tag{12e}$$

Using (12a) in (7a) yields the plane strain balance of forces equations

$$\frac{\partial \sigma_{xx}}{\partial x} + \frac{\partial \sigma_{xy}}{\partial y} = 0 \tag{13a}$$

$$\frac{\partial \sigma_{yy}}{\partial y} + \frac{\partial \sigma_{xy}}{\partial x} = 0 \tag{13b}$$

with the boundary conditions

$$\sum_j \sigma_{ij} u_j = 0 \qquad i, j = 1, 2. \tag{14}$$

As noted above the existence of the function $\bar{U}$ requires a compatibility relationship between strain, and therefore stress, components. By direct substitution of (5) it is clear that the strain components must satisfy the compatibility relations

$$\frac{\partial^2 \epsilon_{ii}}{\partial x_j^2} + \frac{\partial^2 \epsilon_{jj}}{\partial x_i^2} = 2\frac{\partial^2 \epsilon_{ij}}{\partial x_i \partial x_j}. \tag{15}$$

Under the plane strain approximation (15) becomes

$$\frac{\partial^2 \epsilon_{yy}}{\partial x^2} + \frac{\partial^2 \epsilon_{xx}}{\partial y^2} = 2\frac{\partial^2 \epsilon_{xy}}{\partial x \partial y}. \tag{16}$$

Using (12a)-(12c) in (16) to eliminate the strain components yields the stress compatibility equation

$$\left(\frac{\partial^2}{\partial y^2} + \frac{\partial^2}{\partial x^2}\right)\left(\sigma_{xx} + \sigma_{yy} + \frac{E\alpha T'}{1-\nu}\right) = 0. \tag{17}$$

This equation, along with (13a) and (13b) and the boundary conditions (14), uniquely determines the stress distribution and is equivalent to the solution specified by (9) and (10) for the two-dimensional case.

D. The Airy Stress Potential

The Airy stress potential [18] is very useful for solving two-dimensional stress problems. It reduces the problem from a set of two coupled partial differential equations for two functions to a single fourth-order partial differential equation for a single function.

The Airy stress potential ϕ is defined by its relationship to the stress components

$$\sigma_{xx} = \frac{\partial^2 \phi}{\partial y^2} \tag{18a}$$

$$\sigma_{yy} = \frac{\partial^2 \phi}{\partial x^2} \tag{18b}$$

$$\sigma_{xy} = \frac{\partial^2 \phi}{\partial x \partial y}. \tag{18c}$$

With this definition it is readily shown that the two-dimensional balance of forces equations (13) are satisfied for any choice of ϕ. The compatibility relationship becomes

$$\left\{\frac{\partial^4}{\partial x^4} + 2\frac{\partial^4}{\partial x^2 \partial y^2} + \frac{\partial^4}{\partial y^4}\right\}\phi(x, y) = -\frac{E\alpha}{1-\nu}\left\{\frac{\partial^2}{\partial x^2} + \frac{\partial^2}{\partial x^2}\right\}T(x, y) \tag{19}$$

with the boundary conditions

$$u_x \frac{\partial^2 \phi}{\partial x^2} + u_y \frac{\partial^2 \phi}{\partial x \partial y} = 0$$

and

$$u_y \frac{\partial^2 \phi}{\partial y^2} + u_x \frac{\partial^2 \phi}{\partial x \partial y} = 0. \tag{20}$$

Notice that if ϕ is a solution of (19) satisfying (20) on the boundaries, then $\phi + a + bx + cy$ is also a solution. Thus, it is necessary to specify ϕ at three different points to uniquely determine the solution. We are, however, guaranteed that a unique solution does exist. There are methods for solving problems of this type [20] and for our purposes it is assumed that the Airy stress potential, and thus the stress distribution, is known. The strain distribution may be determined from Hooke's law, if desired. The displacement function $\bar{U}(x, y)$ may be calculated from the strain distribution (see Appendix A).

This completes the formulation of temperature and stress distributions in a solid medium.

E. Solutions for Rod and Slab Geometries

In this section we use the results developed in the previous section to find the temperature and stress distributions for a uniformly pumped rod and slab. The thermally induced stress is compared with the material fracture limit to derive an expression for the stress fracture limit. The stress and temperature distributions are used in a following section to determine focusing and birefringence in the thermally stressed rod and slab.

1) Temperature and Stress Distribution in a Uniformly Pumped Rod: Due to the symmetry of the rod it is useful to calculate the temperature and stress distribution in a cylindrical coordinate system.

a) Temperature: The heat flow equation, (3), in a cylindrical coordinate system is

$$\nabla^2 T(r) = \left(\frac{1}{r}\frac{\partial}{\partial r} r \frac{\partial}{\partial r}\right) T(r) = -\frac{Q(r)}{k} \tag{21}$$

with the boundary conditions

$$k\frac{\partial T}{\partial r}\bigg|_{d/2} = \lambda[T_c - T(d/2)] \tag{22}$$

where T_c is the coolant temperature and d is the diameter of the rod. If the rod is uniformly pumped, then Q is a constant. The solution for constant Q is

$$T = T_a + \left(\frac{Q}{4k}\right)\left[\frac{1}{2}\left(\frac{d}{2}\right)^2 - r^2\right]$$

where

$$T_a = T_c + \frac{Qd}{4\lambda} + \frac{Q}{8k}\left(\frac{d}{2}\right)^2. \tag{23}$$

b) Stress: The Airy stress function satisfies (19) and (20). However, due to the circular symmetry of the problem, ϕ is a function of r only and the stresses reduce to $\sigma_{rr}(r)$ and $\sigma_{\theta\theta}(r)$, where σ_{rr} is the stress along the radial axis and $\sigma_{\theta\theta}$ is the stress along the aximuthal axis. The stress along the z-axis, σ_{zz}, is then obtained from (12b).

In cylindrical coordinates, with no θ dependence, the Airy stress potential is the solution of (19) written in cylindrical coordinates,

$$\frac{1}{r}\frac{\partial}{\partial r} r \frac{\partial}{\partial r}\frac{1}{r}\frac{\partial}{\partial r} r \frac{\partial}{\partial r}\phi(r) = \frac{E\alpha Q}{(1-\nu)k} \tag{24}$$

satisfying the boundary conditions

$$\frac{1}{r}\frac{\partial}{\partial r}\phi(r)\,|_{r=d/2} = 0. \tag{25}$$

The radial and tangential stress components from (18) are given by

$$\sigma_{rr} = \frac{1}{r}\frac{\partial\phi}{\partial r}$$

$$\sigma_{\theta\theta} = \frac{\partial^2\phi}{\partial r^2}. \tag{26}$$

The solution of these equations is

$$\Phi = \frac{Q}{16M_s}\left[\frac{r^4}{4} - \frac{d^2r^2}{8}\right]$$

$$\sigma_{rr} = \frac{Q}{16M_s}\left[r^2 - \frac{d^2}{4}\right]$$

$$\sigma_{\theta\theta} = \frac{Q}{16M_s}\left[3r^2 - \frac{d^2}{4}\right]$$

$$\sigma_{zz} = \frac{Q}{8M_s}\left[2r^2 - \frac{d^2}{4}\right] \tag{27}$$

where the material constant M_s is given by

$$M_s = \frac{(1-\nu)k}{\alpha E}. \tag{28}$$

c) Stress Fracture Limit: The mechanical properties of the laser host material determine the maximum surface stress that can be tolerated prior to fracture. If there were no other constraints, such as stress induced focusing and birefringence, the thermal loading and thus average output power of a rod laser could be increased until stress fracture occurred. If we let $\sigma_{\max}$ be the maximum surface stress at which fracture occurs, then we can introduce a steady state thermal stress resistance parameter R_s given by [21]

$$R_s = \sigma_{\max} M_s \tag{29}$$

where M_s is the material parameter given by (28). If $\sigma_{\max}$ is known, then R_s is a stress fracture material figure of merit. Unfortunately, $\sigma_{\max}$ is known for only a few materials, and it is, therefore, useful to use M_s as a material figure of merit for material comparisions. Besides $\sigma_{\max}$ is not well determined since it depends strongly on the surface quality and preparation procedures.

Note that (27) shows that on the surface of a rod $\sigma_{rr} = 0$, and that $\sigma_{\theta\theta}$ and σ_{zz} are equal. The surface stress, σ_s, is

$$\sigma_s = \frac{Q}{32\,M_s}d^2. \tag{30}$$

The stress fracture limit occurs when $\sigma_s = \sigma_{\max}$. Rewriting Q in terms of the thermal loading per unit length P_a/l, where P_a is the total thermal power absorbed by the rod, the maximum power loading of a rod at the stress fracture limit is given by

$$\frac{P_a}{l} = 8\pi R_s \tag{31}$$

Note that the maximum thermal loading is independent of the rod diameter.

2) Temperature and Stress Distribution in a Uniformly Pumped Slab of Infinite Extent: A slab of infinite extent is defined such that the width, or the dimension in the x direction, is of infinite extent. For homogeneous thermal loading the heat flow is only in the y direction and σ_{yy} is zero everywhere.

a) Temperature: Heat flow in an infinite slab with constant heat input per unit volume Q is a one-dimensional problem. The thermal equation and boundary conditions are

$$\nabla^2 T = \frac{\partial^2 T}{\partial y^2} = -\frac{Q}{k} \tag{32a}$$

$$\frac{\partial T}{\partial y}\bigg|_{y=\pm t/2} = \frac{\lambda}{k}[T_c - T(y = \pm t/2)] \tag{32b}$$

where t is the slab thickness, as shown in Fig. 1(a) and T_c is the coolant temperature. These equations have the solution

$$T(y) = T_a + T'(y)$$

where

$$T'(y) = \frac{Qt^2}{8k}\left[\frac{1}{3} - \left(\frac{2y}{t}\right)^2\right]$$

and

$$T_a = T_c + \frac{Qt}{2}\left(\frac{1}{\lambda} + \frac{t}{6k}\right). \tag{33}$$

b) Stress: By symmetry the Airy stress function must be independent of x. In addition, the yy component of stress, σ_{yy}, is zero everywhere. Since by symmetry ϵ_{xx} equals ϵ_{zz}, which is zero, (12b) and (12c) give

$$\sigma_{xx} = \frac{E\alpha}{(1-\nu)}T'(y) = \frac{Q}{2M_s}\left[y^2 - \frac{t^2}{12}\right]$$

$$\sigma_{zz} = \sigma_{xx} \tag{34}$$

where M_s is the material constant given by (28).

c) Stress Fracture Limit: The stress fracture limit was defined above for the rod case. By analogy the stress fracture limit for

a slab of infinite extent occurs when the surface stress σ_s equals the surface fracture stress $\sigma_{\max}$.

The surface stress for the slab is

$$\sigma_s = \frac{Q}{12M_s} t^2. \tag{35}$$

Stress fracture at the surface limits the total thermal power absorbed by the slab per unit of face area. For slabs of finite width W, the power per unit length at the stress fracture limit is given by

$$P_a/l = 12R_s \left(\frac{w}{t}\right) \tag{36}$$

where w/t is the aspect ratio of a finite slab.

It is interesting to compare the surface stress of a rod and slab at equivalent thermal loading per unit volume. From (30) and (35) we find

$$\frac{(\sigma_s)_{\text{rod}}}{(\sigma_s)_{\text{slab}}} = \frac{3}{8}\left(\frac{d}{t}\right)^2. \tag{37}$$

The ratio of thermal power absorbed per unit length at the stress fracture limit from (31) and (36) is given by

$$\frac{(P_a/l)_{\text{rod}}}{(P_a/l)_{\text{slab}}} = \frac{2\pi}{3}\left(\frac{t}{w}\right). \tag{38}$$

Thus, for superior power handling capability relative to a rod, the aspect ratio of the slab must be greater than two.

III. Optical Propagation

A. Introduction

The temperature and stress induced effects on optical propagation are introduced in this section. The discussion considers isotropic media as a special case, but is valid also for crystalline media. The temperature and stress distributions are assumed to be known in the region of interest.

If an isotropic material is subject to thermal stress, there is a direct modification of the index of refraction due to the temperature change, and a modification due to the stress induced by the temperature gradient. In an isotropic medium the index of refraction becomes a second rank tensor $\bar{\bar{n}}$, whose components are given by

$$n'_{ij} = n_0 + \frac{dn_0}{dT} T' + \sum_{kl} B_{ijkl}\, \sigma_{kl} \tag{39}$$

where dn_0/dT is the change in the index of refraction with temperature, the B_{ijkl} are the components of the fourth rank stress optic tensor, $\bar{\bar{B}}$, and the σ_{kl} are the components of the second rank stress tensor. (See Appendix B.)

In an isotropic medium, the stress optic tensor $\bar{\bar{B}}$ must be invariant under spatial rotation and under inversion [22]. This requirement greatly restricts the number of nonzero independent stress optical coefficients. If the reduced notation [22]

$$1 = xx;\quad 2 = yy;\quad 3 = zz;\quad 4 = zy;\quad 5 = zx;\quad 6 = yx$$

is used, then the only nonzero stress optical coefficients are

a) $B_{11} = B_{22} = B_{33} \equiv B_{\parallel}$

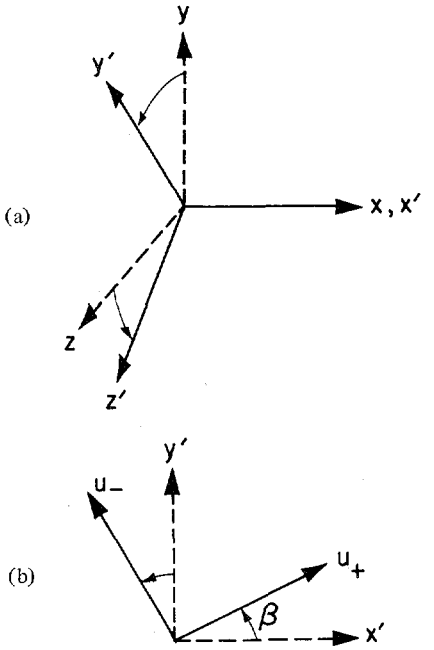

Fig. 2. Optical coordinate systems in the slab. (a) The x, y, z coordinate system is the slab coordinate system shown in Fig. 1. Optical rays propagate along the z axis which is at an angle θ with respect to the slab z axis and in the slab y-z plane. (b) The polarization eigenvectors u_+, u_- form a coordinate system at an angle β with respect to the optical ray x-y coordinate system.

b) $B_{12} = B_{21} = B_{13} = B_{31} = B_{23} = B_{32} \equiv B_{\perp}$

c) $B_{44} = B_{55} = B_{66} \equiv B_{\parallel} - B_{\perp}$

where $B_{\parallel}$ and $B_{\perp}$ give the change in the optical index for stress applied parallel and perpendicular to the polarization axis, respectively. Note that $B_{\parallel}$ and $B_{\perp}$ are the only independent stress optic coefficients in an isotropic medium.

In anisotropic media there are more than two independent stress optic coefficients. A cubic material, such as YAG, has three independent coefficients. The equations derived in this section do not depend explicitly on the form of $\bar{\bar{B}}$ and thus the results can be extended to the crystalline media case.

For the case of optical propagation along a zig-zag optical path, at an angle θ with respect to the z axis and in the y-z plane, it is convenient to rotate the index of refraction tensor $\bar{\bar{n}}$ into a primed coordinate system with the z' axis at an angle θ to the z axis as shown in Fig. 2(a). For propagation straight through a rod or a slab, θ is zero.

The components of the index tensor in the primed reference frame, n''_{ij} are given by

$$n''_{ij} = \sum_{kl} R_{ijkl}\, n'_{kl} \tag{40}$$

or in matrix form

$$\bar{\bar{n}}'' = \bar{\bar{R}}(\theta)\, \bar{\bar{n}}'\, \bar{\bar{R}}(-\theta) \tag{41}$$

where the rotation matrix $\bar{\bar{R}}(\theta)$ is given by

$$\bar{\bar{R}}(\theta) = \begin{vmatrix} 1 & 0 & 0 \\ 0 & \cos\theta & \sin\theta \\ 0 & -\sin\theta & \cos\theta \end{vmatrix}. \tag{42}$$

The submatrix of $\bar{\bar{n}}''$ perpendicular to the direction of optical propagation, denoted by

$$n_{\perp}'' = \begin{vmatrix} n_{xx}'' & n_{xy}'' \\ n_{xy}'' & n_{yy}'' \end{vmatrix} \tag{43}$$

has eigenvalues given by

$$n_{\pm} = \tfrac{1}{2}\{(n_{xx}'' + n_{yy}'') \pm [(n_{xx}'' - n_{yy}'')^2 + 4n_{xy}''^2]^{1/2}\}. \tag{44}$$

The eigenvalues are real for any choice of n_{xx}'', n_{yy}'', or n_{xy}''. Thus the eigenvectors correspond to real directions which are labeled as the $\hat{u}_+$ axis and the $\hat{u}_-$ axis. The indexes of refraction for plane waves linearly polarized along the $\hat{u}_+$ and $\hat{u}_-$ axis are n_+ and n_-, respectively.

Let β be the angle between the x' axis and the $\hat{u}_+$ axis as shown in Fig. 2(b), then

$$\tan\beta = \frac{n_+ - n_{xx}'}{n_{xy}'} \qquad (n_{xx}' < n_{yy}')$$

$$\cot\beta = \frac{n_+ - n_{yy}'}{n_{xy}'} \qquad (n_{xx}' > n_{yy}'). \tag{45}$$

The equation governing optical propagation for a plane wave propagating in the z' direction is given by

$$\frac{1}{ik_v}\frac{\partial}{\partial z'}\begin{bmatrix} E_+(z') \\ E_-(z') \end{bmatrix} = \begin{bmatrix} n_+ & 0 \\ 0 & n_- \end{bmatrix}\begin{bmatrix} E_+(z') \\ E_-(z') \end{bmatrix} \tag{46}$$

where k_v is 2π times the inverse vacuum wavelength.

The solution is

$$\begin{bmatrix} E_+(z') \\ E_-(z') \end{bmatrix} = e^{ik_v n_a z'}\begin{bmatrix} e^{ik_v \Delta n_s z'} & 0 \\ 0 & e^{-ik_v \Delta n_s z'} \end{bmatrix}\begin{bmatrix} E_+(0) \\ E_-(0) \end{bmatrix} \tag{47}$$

where $n_a = (n_+ + n_-)/2$ and $\Delta n_s = (n_+ - n_-)/2$. Since we consider waves polarized along the y' and $x' = x$ axis, it is useful to rotate this result into the x'-y' frame. Since

$$\begin{bmatrix} E_x \\ E_y \end{bmatrix} = \bar{\bar{R}}(-\beta)\begin{bmatrix} E_+ \\ E_- \end{bmatrix} = \begin{bmatrix} \cos\beta & -\sin\beta \\ \sin\beta & \cos\beta \end{bmatrix}\begin{bmatrix} E_+ \\ E_- \end{bmatrix} \tag{48}$$

the solution transforms to

$$\begin{bmatrix} E_x(z') \\ E_y(z') \end{bmatrix} = e^{ik_v n_a z'}\,\bar{\bar{R}}(-\beta)\begin{bmatrix} e^{ik_v \Delta n_s z'} & 0 \\ 0 & e^{-ik_v \Delta n_s z'} \end{bmatrix} \cdot \bar{\bar{R}}(\beta)\begin{bmatrix} E_x(0) \\ E_y(0) \end{bmatrix}. \tag{49}$$

During propagation the optical wave or ray suffers a phase change and a polarization modification. The average phase change is given by the overall phase factor $e^{ik_v n_a z'}$ and the polarization modification is given by the product of the three matrices, which is equivalent to a single Jones matrix [23].

B. Focusing and Birefringence

Equations and approximations developed in the previous section can be used to determine the focusing and birefringence in a rod and slab. We limit the discussion to isotropic media.

1) Rod: Consider first the thermal and stress induced focusing and birefringence in a rod of diameter d. Due to the rod symmetry it is useful to work in a cylindrical coordinate system. In this coordinate system the nonzero components of the index of refraction submatrix perpendicular to the z axis are

$$n_{rr}' = n + \frac{dn}{dT}T'(r) + B_{\perp}[\sigma_{zz}(r) + \sigma_{\theta\theta}(r)] + B_{\parallel}\,\sigma_{rr}(r) \tag{50a}$$

$$n_{\theta\theta}' = n + \frac{dn}{dT}T'(r) + B_{\perp}[\sigma_{zz}(r) + \sigma_{rr}(r)] + B_{\parallel}\,\sigma_{\theta\theta}(r) \tag{50b}$$

where n is the unperturbed index of refraction. Since the only nonzero elements are the diagonal elements, they are also the eigenvalues of the matrix. The eigenvectors are thus along the radial axis and the azimuthal axis.

Using the temperature distribution given by (23) and the stress distributions given by (27), the indexes of refraction may be written as

$$n_r = n^0\left(1 - \frac{\alpha_r}{2}r^2\right) \tag{51a}$$

$$n_\theta = n^0\left(1 - \frac{\alpha_\theta}{2}r^2\right) \tag{51b}$$

where

$$n^0 = n + \frac{dn}{dT}\frac{Q}{8k}\left(\frac{d}{2}\right)^2 - \frac{Q}{16M_s}[3B_{\perp} + B_{\parallel}] \tag{52}$$

and

$$\alpha_r \equiv \frac{2}{n^0}\left\{\frac{dn}{dT}\frac{Q}{4k} - \frac{Q}{16M_s}(7B_{\perp} + B_{\parallel})\right\} \tag{53a}$$

$$\alpha_\theta \equiv \frac{2}{n^0}\left\{\frac{dn}{dT}\frac{Q}{4k} - \frac{Q}{16M_s}(5B_{\perp} + 3B_{\parallel})\right\}. \tag{53b}$$

The index of refraction distribution for the radial and azimuthal polarizations is approximately that of a lens-like medium with index of refraction gradient parameters α_r and α_θ. Ray matrices for lens-like media are well known [24], [25]. If $\alpha_r l^2 \ll 1$ and $\alpha_\theta l^2 \ll 1$, where l is the length of the rod, the ray matrix for propagation through the rod is equivalent to the ray matrix for a biaxial thin lens combined with a propagation distance l. The focal lengths of the biaxial thin lens are

$$f_r = \frac{1}{n^0 l\alpha_r} \tag{54a}$$

$$f_\theta = \frac{1}{n^0 l\alpha_\theta} \tag{54b}$$

for radially and azimuthally polarized light, respectively.

Within a laser resonator the strong biaxial lens element degrades the optical quality of the fundamental mode and induces additional cavity loss [1]-[4]. Since a biaxial lens does not have a unique image plane, radiation which passes through an aperture on one pass cannot be reimaged through the aperture on the next pass, thus inducing loss in the cavity. Beyond a certain thermal loading level, the induced loss increases faster than the round trip gain and laser oscillation can be extinguished by the thermally induced biaxial lens.

The biaxial focal power can be expressed as the difference between the radial and tangential focal powers. This focal power represents the uncorrectable focusing of the rod. The biaxial focal power is defined by

$$\frac{1}{f_b} = \frac{1}{f_\theta} - \frac{1}{f_r}. \tag{55}$$

Substituting (53) and (54) into (55) yields

$$\frac{1}{f_b} = \frac{lQ}{4M_s}\left[B_\perp - B_\parallel\right] \tag{56}$$

where $B_\perp - B_\parallel$ is recognized as the stress optic coefficient ΔB.

Rewriting Q in terms of the absorbed thermal power $P_a = Q \cdot V$, where V is the volume of the rod, gives

$$\frac{1}{f_b} = \frac{P_a}{\pi d^2 M_s}\left[B_\perp - B_\parallel\right]. \tag{57}$$

Note that the biaxial focusing is independent of the length of the rod at constant input power.

Not only do the optical beams suffer biaxial focusing, they also suffer position dependent depolarization. This depolarization is most easily analyzed by considering rays propagating through the rod and ignoring diffraction effects. A ray, R, traveling through the rod parallel to the z axis at position (r) and propagating according to (46) suffers a phase delay between the entrance plane ($z = 0$) and exit plane ($z = l$) that depends on the position and polarization of the ray. In the (r) coordinate system the solution to (46) is

$$\begin{bmatrix} R_r(l) \\ R_\theta(l) \end{bmatrix} = e^{ik_v n_a l} \begin{vmatrix} e^{ik_v \Delta n_s l} & 0 \\ 0 & e^{-ik_v \Delta n_s l} \end{vmatrix} \begin{bmatrix} R_r(0) \\ R_\theta(0) \end{bmatrix}$$

with

$$n_a(r) = n_0\left(1 - \frac{\alpha_r + \alpha_\theta}{4} r^2\right)$$

and

$$\Delta n_s(r) = n_0(\alpha_\theta - \alpha_r)\frac{r^2}{4} = \frac{Qr^2}{16M_s}\left[B_\perp - B_\parallel\right]. \tag{58}$$

In the x-y coordinate system, the solution transforms to

$$\begin{bmatrix} R_x(l) \\ R_y(l) \end{bmatrix} = e^{ik_v n_a l} \begin{bmatrix} \cos^2\theta e^{i\gamma} + \sin^2\theta e^{-i\gamma} & -i\sin 2\theta \sin\gamma \\ -i\sin 2\theta \sin\gamma & \cos^2\theta e^{-i\gamma} + \sin^2\theta e^{i\gamma} \end{bmatrix} \begin{bmatrix} R_x(0) \\ R_y(0) \end{bmatrix}$$

where the propagation constant γ is defined by

$$\gamma \equiv k_v \Delta n_s l. \tag{59}$$

If a ray, initially polarized in the x direction, propagates through the rod, its intensity after passing through an analyzer oriented to transmit the x polarization is given by

$$|R_x(l)|^2 = [1 - \sin^2(2\theta)\sin^2\gamma(r)]\,|R_x(0)|^2. \tag{60}$$

For large Q, such that $\gamma(d/2) \gtrsim \pi/2$, the rod distorts the intensity pattern of polarized optical beams as well as causes biaxial focusing. Note that the magnitude of the effect depends upon the product of the power density and the length. Thus, increasing the overall length while proportionally decreasing the power density does not improve the performance. In rod geometry lasers, stress induced birefringence restricts the average power output from a polarized laser oscillator to a level well below the average power set by biaxial focusing and stress fracture.

2) Slab of Infinite Extent: In the Cartesian coordinate system appropriate for the slab symmetry, the nonzero components of the index of refraction tensor are

$$n_{xx} = n + \frac{dn}{dT}T'(y) + B_\perp\sigma_{zz} + B_\parallel\sigma_{xx} \tag{61a}$$

$$n_{yy} = n + \frac{dn}{dT}T'(y) + B_\perp(\sigma_{zz} + \sigma_{xx}) \tag{61b}$$

$$n_{zz} = n_{xx}. \tag{61c}$$

For a beam propagating straight through the slab parallel to the z axis, the submatrix perpendicular to the axis of propagation is already diagonal. The indexes of refraction are given by (61) with temperature and stress distribution from (33) and (34). Thus

$$n_x = n_x^0\left(1 - \frac{\alpha_x}{2}y^2\right) \tag{62a}$$

$$n_y = n_y^0\left(1 - \frac{\alpha_y}{2}y^2\right) \tag{62b}$$

where

$$n_x^0 = n + \frac{dn}{dT}\frac{Qt^2}{24k} - \frac{Qt^2}{24M_s}(B_\perp + B_\parallel) \tag{63a}$$

$$n_y^0 = n + \frac{dn}{dT}\frac{Qt^2}{24k} - \frac{Qt^2}{12M_s}B_\perp \tag{63b}$$

with

$$\alpha_x = \frac{2}{n_x^0}\left\{\frac{dn}{dT}\left(\frac{Q}{2k}\right) - \frac{Q}{2M_s}(B_\perp + B_\parallel)\right\} \tag{64a}$$

$$\alpha_y = \frac{2}{n_y^0}\left\{\frac{dn}{dT}\left(\frac{Q}{2k}\right) - \frac{Q}{M_s}B_\perp\right\}. \tag{64b}$$

The index of refraction distribution for the x or y polarizations is approximately that of a cylindrical lens-like medium.

If $\alpha_x l^2 \ll 1$ and $\alpha_y l^2 \ll 1$, where l is the length of the slab, then the ray matrix for propagation through the slab is equiva-

lent to the ray matrix for a birefringent cylindrical lens combined with a propagation distance l. The focal lengths of the birefringent lenses are

$$f_x = \frac{1}{n_x^0 \, l \, \alpha_x} \tag{65a}$$

$$f_y = \frac{1}{n_y^0 \, l \, \alpha_y} \tag{65b}$$

for x and y polarized light, respectively. The thermal and stress induced focusing for propagation straight through the slab is correctable and is linear in the input power.

Comparing (54) for the focal length of a rod with (65) for the focal lengths of a slab, shows that when thermal focusing is greater than stress induced focusing, which is the case for glasses with nonzero dn/dT, then the slab has twice the focal power of a rod. For the special case where $dn/dT = 0$ and only stress induced focusing is important, the slab still has approximately twice the focal power of the rod. We show below that the zig-zag path eliminates focusing in the slab.

The rectilinear infinite slab, by the symmetry arguments given above, has stress tensor components that satisfy the equality $\sigma_{zz} = \sigma_{xx}$ in addition to $\sigma_{yy} = 0$. Thus for incident radiation polarized along either the x or y direction the stress induced depolarization is zero.

C. The Zig-Zag Optical Path

1) Introduction: In the previous section we considered propagation straight through an infinite slab. This choice of laser medium symmetry eliminated stress induced biaxial focusing and depolarization. However, the focusing along one axis of the slab was increased by about a factor of two relative to that of a rod. The focusing in the slab can be eliminated by choosing to propagate along a zig-zag optical path. In the zig-zag geometry, the optical beam does not travel parallel to the z axis, as was the case for the straight-through optical path. Instead the beam traverses the slab at an angle with respect to the x-z plane using total internal reflection from the slab y faces. This geometry is shown in Fig. 3. The zig-zag optical beam path can be achieved by refraction from the input window of the slab, as shown in Fig. 3(a), or by orienting the slab at an angle with respect to the direction of the incoming beam as shown in Fig. 3(b). It should be noted that the zig-zag path can also be achieved through external reflecting surfaces as is done in active mirror amplifier designs.

2) Depolarization: Since the zig-zag optical beam path is no longer parallel to the slab z axis, the question arises as to whether the Jones matrix for propagation through the slab is still diagonal in the optical beam x-y frame. The matrix for transmittance through the slab's input window is diagonal in the x-y frame because the x axis is parallel to the input plane. The matrix for total internal reflection from the side surfaces is also diagonal in the x-y frame because the x axis is parallel to the plane of the side surfaces. Since the refractive index tensor in an infinite slab is diagonal in the slab x-y-z frame, a rotation about the x axis yields a new tensor whose submatrix, perpendicular to the new z axis, is also diagonal in the new x-y frame. Thus, all of the component parts of the Jones matrix for propagation through the slab are diagonal in the zig-zag optical beam x-y frame. Therefore, we conclude that the Jones matrix for propagation through the slab must also be diagonal in the zig-zag optical beam x-y frame and thus properly polarized beams suffer no depolarization.

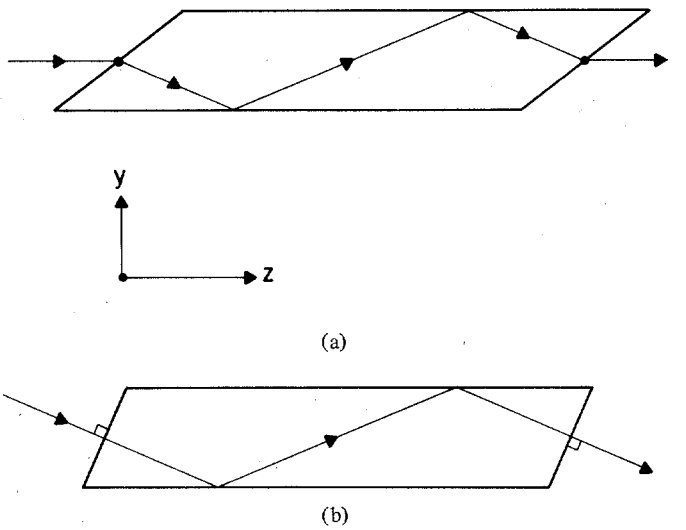

Fig. 3. The zig-zag slab geometry for (a) rays refracted at the input face of the slab and reflected by total internal reflection at the slab y = constant faces, and (b) rays transmitted near normal to the input faces.

In practice, slab configured laser media only approximate the ideal infinite slab thus far assumed. In slab media of finite extent σ_{yy} is not zero everywhere and numerical calculations must be performed to determine σ_{yy} and the resulting stress induced depolarization. The discussion of such a numerical analysis and results are presented in Part II of this paper. However, we anticipate the results by noting that in a 3:1 aspect ratio glass slab, thermally loaded to the stress fracture limit, the peak depolarization calculated using our model is 30 percent near the uncooled edge while the average depolarization over the entire area of the slab is less than 3 percent. Thus, the slab configuration shows significantly reduced depolarization compared to a thermally loaded rod geometry media.

3) Focusing: In the zig-zag optical path all undeflected rays suffer the same average phase retardation due to thermal effects. Thus the zig-zag optical path eliminates first-order focusing effects.

A more detailed ray tracing analysis has been performed [13] and confirms this argument. A result of the ray tracing analysis shows that the optical phase distortion induced by the slab is proportional to $l^3 \alpha_y^2 / N^2$ where N is the number of bounces in the slab and α_y is given by (64b). For reasonable slab geometries, the second-order focusing effects are not significant until the input power exceeds the stress fracture limit by more than one order of magnitude.

Focusing effects linear in the pump power in zig-zag optical path slab geometry lasers can arise from three different effects. Under thermal loading the induced stress leads to surface bulge. Since the optical path includes reflections from two of these surfaces this bulge causes focusing effects. Furthermore, the bulging of the entrance and exit faces and index gradients in these regions cause beam focusing. Direct flashlamp pumping of the entrance and exit faces is not recommended as this causes

a significant focusing effect. These effects are present in rod laser systems, but are usually insignificant compared to the bulk focusing.

These surface bulge and end effects are measurable in slab laser systems due to the absence of the bulk focusing effects. Both effects are correctable in the central region of the slab. Focusing may also arise from nonuniform pumping or cooling of the slab. Care must be taken to ensure that the reflector structure uniformly illuminates the slab and that the cooling geometry maintains a nearly constant surface temperature on the slab. The arguments presented here apply to an infinite slab and thus, neglect boundary effects. Focusing due to surface curvature induced by stress is also neglected. These effects are not easily treated analytically but can be calculated by the numerical methods that are described in Part II of this paper.

The zig-zag path eliminates first-order thermal and stress induced focusing in the thermally loaded infinite slab. The elimination of both birefringence and focusing by use of the zig-zag slab geometry permits the design of high-power solid-state lasers that are performance limited by stress fracture of the medium.

IV. Slab Laser Scaling Laws

A. Introduction

It is very useful in a laser design process to have scaling laws for parameters that affect the laser performance. In this section scaling laws for slab geometry lasers are considered.

B. Temperature and Stress

The temperature profile in the central region of the slab is assumed to be equivalent to that of the infinite slab temperature distribution given by

$$T(x, y) = \frac{Qt^2}{8k}\left[\frac{1}{3} - (2y/t)^2\right] + T_a. \tag{66}$$

Here $T(x, y)$ is the temperature distribution in the slab, T_a is the average temperature of the slab, k is the thermal conductivity, and t is the slab thickness. If the end faces are not perfectly insulated, the temperature distribution deviates from the infinite slab model near the end faces. This deviation decreases exponentially with distance from the side face with a characteristic length of half the slab thickness.

The stress on the reflecting surface of the slab can also be determined from the infinite slab model. The surface stress σ_s is given by

$$\sigma_s = \frac{1}{12}\frac{Q}{M_s}t^2 \tag{67}$$

where the material parameter M_s is defined by (28).

The surface stress can be expressed in terms of a temperature difference ΔT between the center of the slab ($y = 0$) and the y face ($y = t/2$) using (66) in (67) by

$$\sigma_s = \frac{2}{3}\frac{k}{M_s}\Delta T. \tag{68}$$

Thus, the surface stress depends on the temperature difference and is independent of the average temperature of the slab T_a. In operation, the surface stress σ_s must be maintained at a safe level below the fracture stress $\sigma_{\max}$ to prevent fracture of the slab.

C. Gain, Repetition Rate, and Average Power

The gain in the slab is determined by the stored upper level energy density, E_{st}. The heat generated in the slab arises from quantum inefficiencies and the quantum defect in converting pump photons into excited state population. The stored upper state energy density per flashlamp pulse can be related to Q by

$$Q = E_{st}R\chi \tag{69}$$

where R is the repetition rate and χ is the ratio of the energy dissipated as heat to the energy stored in the upper level of the laser medium. For typical Nd:Glass and Nd:YAG flashlamp pumped lasers χ lies between 1 and 2 and depends on flashlamp current density, spectral filtering, and pulse length.

The unsaturated single-pass gain is given by

$$G_0 = \exp\left(\frac{E_{st}l_p}{E_{\text{sat}}}\right) = \exp(g_0 l_p) \tag{70}$$

where E_{sat} is the saturation fluence, l_p is the path length of the beam through the gain medium, and g_0 is the unsaturated gain coefficient.

Assuming operation at one half the stress fracture limit, the repetition rate is given by

$$R = \frac{1}{E_{\text{sat}}\ln(G_0)}\frac{1}{\chi}[6M_s\sigma_{\max}]\frac{l_p}{t^2} \tag{71}$$

where (70) has been used along with (67a and 67b). The total optical energy stored in the slab per flashlamp pulse, $J = E_{st}V$, is

$$J = E_{\text{sat}}\ln(G_0)\frac{lwt}{l_p}. \tag{72}$$

The average power extracted from a slab laser at the extraction efficiency η_{ex} is given by

$$P_{\text{out}}^{\text{ave}} = JR\eta_{ex} = \frac{6\eta_{ex}R_s}{\chi}\left(\frac{lw}{t}\right) \tag{73}$$

where R_s is the material figure of merit given in (29). Thus, the average output power of a stress fracture limited slab laser scales as the product of slab length times width and inversely with slab thickness. This can be compared with a rod laser which scales linearly with length. The slab offers a potential average power improvement directly proportional to the aspect ratio w/t.

V. Conclusion

In this paper we have presented an analysis of thermal and stress induced effects on optical propagation through a rod, slab, and zig-zag optical path slab medium. The analysis was limited to the case of an infinite rod and slab. The finite slab case, which requires numerical methods of analysis, will be treated in Part II of this paper.

The rod geometry laser average output power is limited in turn by thermal and stress induced birefringence, biaxial focusing, and ultimately by thermal induced stress fracture. In practice, except for special athermal glasses, laser operation is severely hindered by thermal focusing well before the stress fracture limit is reached. Athermal glass still exhibits biaxial stress focusing. If polarized laser output is required for Q-switched operation or for efficient conversion via nonlinear interactions,

thermal induced birefringence sets an even lower average power limit for rod geometry lasers.

In the slab geometry laser, symmetry eliminates stress induced depolarization and the zig-zag optical path cancels first-order focusing. Thus, the zig-zag optical path slab laser can be designed to operate at an average power level limited only by the stress fracture of the laser medium.

Stress calculations show that the thermally induced stress is proportional to the temperature difference between the center of the slab and the cooled faces. The temperature difference in turn scales with the input heat energy per unit volume and the slab thickness squared. Thus long thin slabs offer high average power output without thermal and stress induced focusing or depolarization. Experimental studies, which have confirmed the expected slab geometry advantages, will be presented in Part III of this paper.

The slab geometry offers the important advantage of laser media selection based on laser parameters of interest without the concern for thermal or stress induced focusing. Thus laser media can be selected with good thermal/mechanical properties without regard to dn/dT. This opens the possibility of reconsidering a number of potential laser glass and crystalline hosts that had been rejected earlier as unsuitable for rod geometry lasers because of large thermal focusing effects.

Appendix A

The Displacement Function $U(x, y)$

In this appendix the problem of determining the displacement function $\bar{U}$ from the strain tensor $\bar{\bar{\epsilon}}$ is considered.

In two dimensions, the equations relating strain and displacement are

$$\epsilon_{xx} = \frac{\partial U_x(x, y)}{\partial x} \tag{A.1a}$$

$$\epsilon_{yy} = \frac{\partial U_y(x, y)}{\partial y} \tag{A.1b}$$

$$\epsilon_{xy} = \frac{1}{2}\left(\frac{\partial U_x(x, y)}{\partial y} + \frac{\partial U_y(x, y)}{\partial x}\right). \tag{A.1c}$$

Noting that the equation set is invariant under the exchange of x and y, $U_x(x, y)$ may be found and symmetry used to solve for $U_y(x, y)$. Equations (A.1a) and (A.1b) may be integrated to yield

$$U_x(x, y) = \int_{x_0}^{x} \epsilon_{xx}(x', y)\, dx' + U_x(x_0, y) \tag{A.2a}$$

$$U_y(x, y) = \int_{y_0}^{y} \epsilon_{yy}(x, y')\, dy' + U_y(x, y_0). \tag{A.2b}$$

Using these equations, (A.1c) may be used to yield

$$\frac{\partial U_x}{\partial y}(x_0, y) = 2\epsilon_{xy}(x, y) - \int_{x_0}^{x} \frac{\partial}{\partial y}\epsilon_{xx}(x', y)\, dx' - \int_{y_0}^{y} \frac{\partial}{\partial x}\epsilon_{yy}(x, y')\, dy' - \frac{\partial}{\partial x} U_y(x, y_0). \tag{A.3}$$

Since the left-hand side is independent of x, the right-hand side must also be independent of x, and may therefore be evaluated at $x = x_0$. This new expression is integrated with respect to y to yield

$$U_x(x_0, y) = \int_{y_0}^{y} dy' \left[2\epsilon_{xy}(x_0, y') - \int_{y_0}^{y'} dy'' \left(\frac{\partial}{\partial x}\epsilon_{yy}(x, y'')\Big|_{x=x_0}\right)\right] - \left(\frac{\partial}{\partial x} U_y(x, y)\Big|_{\substack{x=x_0 \\ y=y_0}}\right) y + U_x(x_0, y_0). \tag{A.4}$$

This expression, when combined with (A.2a), yields an expression for $U_x(x, y)$.

Using the x-y symmetry of the basic equation, it is clear that

$$U_y(x, y_0) = \int_{x_0}^{x} dx' \left[2\epsilon_{xy}(x', y_0) - \int_{x_0}^{x'} dx'' \left(\frac{\partial}{\partial y}\epsilon_{xx}(x'', y)\,|_{y=y_0}\right)\right] \cdot \left(-\frac{\partial}{\partial y} U_x(x, y)\Big|_{\substack{x=x_0 \\ y=y_0}}\right) x + U_y(x_0, y_0). \tag{A.5}$$

This expression, when combined with (A.2b), yields an expression for $U_y(x, y)$.

Noting that (A.3c) is valid at the point x_0, y_0, it is seen that there are three independent constants of integration:

1) $U_y(x_0, y_0)$—corresponding to a rigid body translation in the y direction.

2) $U_x(x_0, y_0)$—corresponding to a rigid body translation in the x direction.

3) $\left(\frac{\partial}{\partial x} U_y(x, y) - \frac{\partial}{\partial y} U_x(x, y)\right)\Big|_{\substack{x=x_0 \\ y=y_0}}$—corresponding to a rigid body rotation about the z axis.

Choice of these constants, and the use of (A.1c) and (A.2a), (A.2b), (A.4), and (A.5), yield unique values for $U_x(x, y)$ and $U_y(x, y)$.

Appendix B

Relationship Between the Stress Optic and Index of Refraction Tensors

This paper uses the stress optic tensor $\bar{\bar{B}}$ to calculate the change in the index of refraction resulting from a mechanical stress, according to (39). The coefficients of the tensor $\bar{\bar{B}}$ can be calculated from other tabulated tensors when they are not available directly. These other tensors are the piezo-optic tensor $\bar{\bar{q}}$, the elasto-optic $\bar{\bar{p}}$, and the elastic compliance tensor $\bar{\bar{S}}$. Data for many crystals can be found in Landolt and Bornstein [26].

The piezo-optic tensor $\bar{\bar{q}}$ gives the change in the optical indicatrix, b, due to stress. In the coordinate system that diag-

onalizes the index of refraction tensor, the indicatrix will be diagonal as well, and is given by

$$b_{ii} = \frac{1}{n_{ii}^2} \qquad b_{i \neq j} = 0. \tag{B.1}$$

For a general coordinate system the relation is

$$\sum_{jk} b_{ij} n_{jk} n_{kl} = \delta_{il}. \tag{B.2}$$

The perturbed indicatrix is written in terms of the stress $\bar{\bar{\sigma}}$, the unperturbed indicatrix $\bar{\bar{b}}$, and the piezo-optic tensor according to

$$b_{ij} = b_{ij}^0 + \sum_{kl} q_{ijkl}\, \sigma_{kl}. \tag{B.3}$$

It can be shown that the stress optic tensor $\bar{\bar{B}}$ can be written in terms of $\bar{\bar{q}}$ using the equation

$$B_{ijkl} = -\tfrac{1}{2} \sum_{mnp} n_{im} n_{mn} n_{np} q_{pjkl}. \tag{B.4}$$

For an isotropic material this simplifies to

$$B_{\parallel} = -\tfrac{1}{2}\, n^3\, q_{\parallel}$$
$$B_{\perp} = -\tfrac{1}{2}\, n^3\, q_{\perp}. \tag{B.5}$$

For many crystals, the elasto-optic tensor $\bar{\bar{p}}$ is tabulated. It is used to express changes in the indicatrix proportional to the strain in the crystal, $\bar{\bar{\epsilon}}$. The expression for the perturbed indicatrix in terms of strain is

$$b_{ij} = b_{ij}^0 + \sum_{kl} p_{ijkl} \epsilon_{kl}. \tag{B.6}$$

The tensor $\bar{\bar{q}}$ can be written in terms of $\bar{\bar{p}}$ and the elastic compliance tensor $\bar{\bar{S}}$ according to

$$q_{ijkl} = \sum_{mn} p_{ijmn} S_{mnkl}. \tag{B.7}$$

The values of the various tensors are tabulated in the reduced matrix form, introduced in Section III. This form allows for simple two index tabulation of the four index tensor and allows the relationships between tensors to be replaced by matrix multiplication. Certain factors of two are needed in the transfer from four indexes to two. For the compliance tensor $\bar{\bar{S}}$,

$$\begin{aligned} S_{ijkl} &= S_{mn} && m \text{ and } n \text{ both are } 1, 2, 3 \\ 2S_{ijkl} &= S_{mn} && \text{either } m \text{ or } n \text{ are } 4, 5, 6; \text{ not both} \\ 4S_{ijkl} &= S_{mn} && \text{both } m \text{ and } n \text{ are } 4, 5, 6. \end{aligned} \tag{B.8}$$

For the piezo-optic tensor $\bar{\bar{q}}$

$$\begin{aligned} q_{kjkl} &= q_{mn} && n = 1, 2, 3 \\ 2q_{ijkl} &= q_{mn} && n = 4, 5, 6. \end{aligned} \tag{B.9}$$

For the elasto-optic tensor $\bar{\bar{p}}$

$$p_{kjkl} = p_{mn} \qquad \text{all } m, n. \tag{B.10}$$

For an isotropic material, the values of $B_{\parallel} = B_{11}$ and $B_{\perp} = B_{12}$ can be written in terms of p_{11} and p_{12}, if Poisson's ratio ν and the modulus of elasticity E are known. The relations are

$$B_{\parallel} = \frac{1}{E}(p_{11} - 2\nu p_{12})$$
$$B_{\perp} = \frac{1}{E}[p_{12} - \nu(p_{11} + p_{12})]. \tag{B.11}$$

References

[1] G. D. Baldwin and E. P. Reidel, "Measurements of dynamical optical distortion in Nd:doped glass laser rod," *J. Appl. Phys.*, vol. 38, pp. 2726–2738, 1967.

[2] L. M. Osterink and J. D. Foster, "Thermal effects and transverse mode control and a Nd:YAG laser," *Appl. Phys. Lett.*, vol. 12, pp. 128–131, 1968.

[3] J. D. Foster and L. M. Osterink, "Thermal effects in a Nd:YAG laser," *J. Appl. Phys.*, vol. 41, pp. 3656–3663, 1970.

[4] W. Koechner, "Thermal lensing in a Nd:YAG laser rod," *Appl. Opt.*, vol. 9, pp. 2548–2553, 1970.

[5] W. S. Martin and J. P. Chernoch, "Multiple internal reflection face pumped laser," U.S. Patent 3 633 126, 1972.

[6] J. P. Chernoch, W. S. Martin, and J. C. Almasi, "Performance characteristics of a face pumped, face cooled laser, the mini-FPL," U.S. Air Force Avionics Lab., Wright Patterson Air Force Base, OH, Tech. Reps. AFAL-TR-71-3, 1971.

[7] W. B. Jones, L. M. Goldman, J. P. Chernoch, and W. S. Martin, "The mini-FPL–A face pumped laser: Concept and implementation," *IEEE J. Quantum Electron.*, vol. QE-8, p. 534, 1972.

[8] T. Henningsen, "Evaluation of CaLaSOAP:Nd for use in a one joule, 30 Hz laser designator," Westinghouse Research Lab., Pittsburgh, PA, Res. Rep. 72-1C1-LAMAT-RI, 1972.

[9] J. P. Chernoch, "High power Nd:YAG mini-FPL," U.S. Air Force Avionics Lab., Wright Patterson Air Force Base, OH, Final Rep. AFAL TR-75-93, 1975.

[10] G. J. Hulme and W. B. Jones, "Total internal reflection face pumped laser," in *Proc. Soc. Photo-Optical Instr. Eng.*, vol. 69, pp. 38–45, 1975.

[11] Y. S. Liu, W. B. Jones, and J. P. Chernoch, "Recent development of high power visible laser sources employing solid state slab lasers and nonlinear harmonic conversion techniques," Tech. Rep. 81-CRD104, General Electric Research and Development, Schenectady, NY, 1981.

[12] W. B. Jones, "Face pumped laser with diffraction limited output beam," U.S. Patent 4 214 216, 1980.

[13] J. M. Eggleston, "Theoretical and experimental studies of slab geometry lasers," Ph.D. dissertation, Stanford Univ., Stanford, CA, 1982.

[14] J. M. Eggleston, T. J. Kane, J. Unternahrer, and R. L. Byer, "Slab geometry Nd:glass laser performance studies," *Opt. Lett.*, vol. 9, pp. 405–407, 1982.

[15] T. J. Kane, R. C. Eckardt, and R. L. Byer, "Reduced thermal focusing and birefringence in zig-zag slab geometry crystalline lasers," *IEEE J. Quantum Electron.*, vol. QE-19, 1983.

[16] W. Koechner, *Solid State Laser Engineering* (Springer Series in Optical Sci.). New York: Springer-Verlag, 1976.

[17] D. C. Brown, *High Peak Power Nd:Glass Laser Systems*. New York: Springer-Verlag, 1981.

[18] H. Parker, *Thermal Elasticity*. Waltham, MA: Blaisdell, 1968.

[19] S. P. Timoshenko and J. N. Goodier, *Theory of Elasticity*. San Francisco, CA: McGraw-Hill, 1934, also 1970.

[20] P. E. Bjorstad, "Numerical solution of the biharmonic equation," Ph.D. dissertation, Dep. Comput. Sci., Stanford Univ., Stanford, CA, 1980.

[21] S. W. Freiman, "Fracture mechanics of glass," in *Glass: Science and Technology, Vol. 5, Elasticity and Strength in Glasses*, D. R. Uhlmann and N. J. Kreidl, Eds. New York: Academic, 1980.

[22] J. F. Nye, *Physical Properties of Crystals*. Oxford, England: Oxford Clarendon, 1967.

[23] R. C. Jones, "A new calculus for treatment of optical systems," *J. Opt. Soc. Amer.*, vol. 32, pp. 486–493, 1942.

[24] A. E. Siegman, *Introduction to Lasers and Masers*. New York: McGraw-Hill, 1971.

[25] A. Yariv, *Introduction to Optical Electronics*. New York: Holt, Rinehart, and Winston, 1976.

[26] D. F. Nelson, "Piezo-optic and electro-optic constants of crystals," in *Elastic Piezoelectric, Pyroelectric, Piezo-optic, Electro-optic Constants and Nonlinear Dielectric Susceptibilities of Crystals*, vol. III/11, Landolt-Bornstein, Eds. Berlin, Germany: Springer-Verlag, 1979.

J. M. Eggleston, photograph and biography not available at the time of publication.

T. J. Kane, photograph and biography not available at the time of publication.

K. Kuhn, photograph and biography not available at the time of publication.

J. Unternahrer, photograph and biography not available at the time of publication.

R. L. Byer (M'75), photograph and biography not available at the time of publication.

Velocity-Matching Techniques for Integrated Optic Traveling Wave Switch/Modulators

ROD C. ALFERNESS, STEVEN K. KOROTKY, AND ENRIQUE A. J. MARCATILI, FELLOW, IEEE

Abstract—We propose and analyze a new technique for achieving velocity match between the traveling wave electrical drive and guided optical signal for modulators in substrates for which there is an inherent mismatch. The traveling wave electrodes are laterally shifted periodically to reverse the direction of the applied electric field within the optical waveguide which exactly compensates for the polarity reversal caused by the microwave-optical walkoff. Consequently, the electrooptically induced phase shifts of each section add in phase and several sections can be used to reduce the required drive voltage at the design frequency. This artificial velocity-matching technique moves the mismatch-limited bandwidth to an arbitrarily high design frequency. In addition, we extend the new concept of phase reversal and the previously suggested technique of intermittent interaction by proposing electrode structures with large inactive to active aspect ratios. This generalization provides increased flexibility for manipulating the total available bandwidth to, for example, allow efficient modulation by a train of arbitrarily short electrical pulses. These techniques are ideally suited for several proposed integrated optic devices, including picosecond samplers and gates, which require strong overmodulation at a single high frequency.

I. Introduction

TRAVELING wave integrated optic modulators fabricated in substrate materials for which the optical and microwave velocities are equal offer the potential of very broad modulation bandwidth [1]. However, for important materials such as lithium niobate there is an inherent mismatch between the optical and microwave velocities. As a result, the maximum achievable drive frequency decreases as the modulator length is increased. Conversely, to lower the drive voltage and power, a long device length is required. Thus, a tradeoff must be made between maximum drive frequency and required drive power.

To overcome this material limitation, the concept of effective velocity matching based on device structure or geometry has been proposed for bulk optical modulators. Such velocity-matching schemes are of two types. In the first, which we refer to as real velocity matching, the speeds of the colinear propagating RF and optical signals are made equal. This is generally accomplished by using a two dielectric structure with a significant part of the microwave energy propagating in a material of lower microwave index than the electrooptic substrate [2]. Except for microwave dispersion, the velocity match is broad-band and thus well suited for modulators. However, this technique is generally inefficient because the microwave energy that propagates in the lower index material does not contribute to optical modulation.

The second approach, which is the subject of this paper, we refer to as artificial velocity matching. Although several artificial velocity-matching techniques were proposed for bulk modulators, few successful experimental results have been reported [3]. With the flexibility in design and fabrication of

Manuscript received June 23, 1983.
The authors are with AT&T Bell Laboratories, Holmdel, NJ 07733.

0018-9197/84/0300-0301$01.00